2010 IEEE International Conference on Robotics and Automation
Anchorage Convention District
May 3-8, 2010, Anchorage, Alaska, USA

Selecting Motors for Robots Using Biomimetic Trajectories: Optimum Benchmarks, Windings, and Other Considerations

Jonathon W. Sensinger, *Member, IEEE*

***Abstract*—Robotic actuators must frequently be designed to provide both substantial torque and acceleration in a lightweight package. Their ballistic trajectories require new optimization guidelines, in contrast to constant-speed or low-torque conventional motor design. A framework was derived in this study based on trajectories that incorporated the effect of velocity on torque and acceleration. This framework suggested that speed rate (or mechanical motor constant) was the best benchmark of robotic motor performance. Implications of this framework were evaluated using simulations of 37 optimized motor models. Simulation results confirmed the framework predictions, suggesting that speed rate was a better predictor of motor success than either motor constant or rated power. Optimum winding/gear ratio, supply voltage, and implications for design choices such as continuously variable transmissions are discussed in light of these findings.**

***Index Terms*—Brushless motor, mechanical motor constant, prostheses, speed rate, winding optimization**

I. Introduction

ACTUATORS have been incorporated into commercially available prostheses for the last 40 years [1] and have recently seen promising application in exoskeleton designs [2, 3]. The majority of these devices use electromagnetic motors with gears or hydraulic transmissions, due to their high power density. Although standard commercial motors have been used in the past, increasing attention has been paid to optimized motor windings for particular applications [4, 5]. Fundamental design parameters of electromagnetic motors such as core material, pole placement, and winding arrangement are now being reconsidered to further stretch the limits of performance in prostheses and robots [6].

Robotic motor design has adapted theory and benchmarking parameters from conventional motor design, including such parameters as stall torque (T_s), torque constant (K_t), motor constant (K_m), stall-torque/inertia ratio, power rating ($PR=T_s^2/J_m$, J_m = rotor inertia), and speed rate [7, 8], as well as rated continuous power dissipation. Some of these parameters may be better than others as benchmarks for robotic applications, where large torque, large acceleration, limited range of motion (ROM), and low actuator mass are often required. The importance of these requirements is exemplified in the fields of prosthetics and exoskeletons, where power-supply specifications are constrained since they must be housed within the device. Several of the design teams in the Defense Advanced Research Project Agency's Revolutionizing Prosthetics program have used the utilitarian metric of total mass [9]. This mass includes the mass of the actuator, gear, and most critically, the battery, where the battery is appropriately sized to supply all of the energy required to perform a specific list of parameterized tasks for a given day. By using the energy density of a given battery, energy requirements of different configurations may be easily compared. This total-mass benchmark is useful in comparing isolated configurations, but it cannot guide design choices without running simulations on a specific set of tasks.

The intent of this paper is to evaluate commonly used benchmarks in light of the quasi-ballistic nature of trajectories seen in anthropomorphic and rehabilitation robotics, in an attempt to provide guidelines and equations to minimize motor size and optimize motor windings for a particular robotic application. The speed rate (SR), equal to the reciprocal of the mechanical time constant τ_m, is mathematically shown to be the best benchmark of those considered for trajectories that involve speed, acceleration, and applied torque. An optimization analysis is presented modeling 37 motors, in which supply voltage, windings, gear ratio, and plant gain are optimized, and total mass is calculated, to evaluate the predictive power of the guidelines both in terms of motor success in following the trajectory and total mass minimization.

II. Methods

A. Trajectory profile

In contrast with conventional motors, which are often optimized for constant speed and continuous power dissipation, the majority of rehabilitation robots have almost ballistic trajectories, in which the ROM is rarely more than 180° and the duration ranges from 0.1 to 5 seconds. Prosthesis and exoskeleton trajectories may be modeled after human movement, which is closely approximated by a minimum jerk trajectory [10]. This trajectory provides rapid movement without an abrupt initiation or termination (Fig. 1).

J. W. Sensinger is with the Department of Physical Medicine and Rehabilitation, Northwestern University, and the Neural Engineering Center for Artificial Limbs, Rehabilitation Institute of Chicago, Chicago, IL 60611 (e-mail: sensinger@ieee.org).

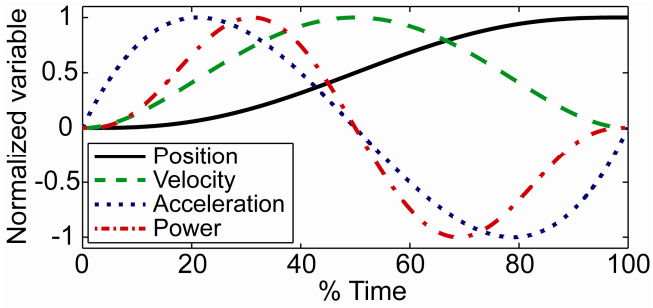

Fig. 1. Normalized kinematics of a minimum jerk trajectory. Minimum jerk trajectories are often used to model human movement and provide a useful model for optimization of motors used in rehabilitation robots.

B. *Derivation of SR as an optimal benchmark*

Any snapshot within the trajectory of a robotic joint may be characterized as a function of velocity, acceleration, and applied torque. The maximum torque a motor may produce at this snapshot is inversely proportional to its speed. The ability of a motor to accelerate an inertial load is accordingly influenced by speed. Simultaneously large speeds and accelerations are often found in biomimetic trajectories (Fig. 1). The available motor torque (T) for output speed ω_p is given by:

$$T = K_t I_{\max}\left(1 - N\omega_p \frac{K_t}{V}\right), \tag{1}$$

where I_{max} is the maximum current, N is the gear ratio, and V is the supply voltage, and assuming stall torque $T_s=K_tI_{max}$, no load speed = V/K_e, and $K_e=K_t$, using SI units.

The torque encountered by the motor (T_p) may be expressed as follows:

$$T_p = \frac{\alpha_p\left(N^2 J_m + J_L\right) + T_L}{N}, \tag{2}$$

where α_p is the acceleration of the output shaft, J_m and J_L are the motor and load inertias, and T_L is the applied load torque.

The relationship between T_s and K_t depends on the value of K_t, the winding resistance, and the properties of the battery (Fig. 2). For smaller K_t, the available current is limited by the battery and T_s is proportional to K_t as expected ($T_s = K_tI_{max}$). For larger K_t, both K_t and I_{max} are dependent on the winding resistance, where I_{max} is limited by the winding resistance to a greater extent than K_t is increased. This dependency results in an inverse relationship between K_t and T_s. The greatest stall torque may be achieved at the intersection of these two regions, when $R_{apx}=V/I_{max}$ (Fig. 2). Winding a motor with greater resistance than R_{apx} reduces efficiency and results in decreased performance. It is therefore not considered for the rest of this paper, although the corollary to the following equations for $R>R_{apx}$ is provided in the appendix. The relationship between K_t and R may be defined using the equation for the motor constant:

$$K_m = \frac{K_t}{\sqrt{R}} \tag{3}$$

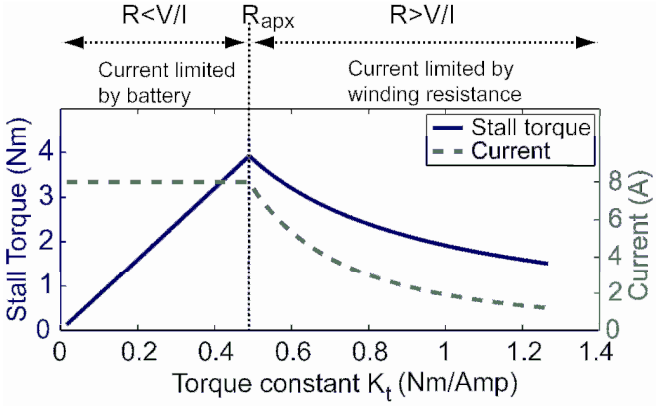

Fig. 2. Stall torque is determined by Kt and current. Above a threshold, increasing Kt decreases the available current, in turn decreasing the stall torque.

If the winding resistance is sufficiently low that I_{max} is a constant, limited by the battery's ability to discharge current (Fig. 2, left side, $R \le R_{apx}$), the required value of K_t may be calculated from (1):

$$K_t^* = \frac{VI_{\max} - \sqrt{VI_{\max}\left(VI_{\max} - 4TN\omega_p\right)}}{2NI_{\max}\omega_p} \tag{4}$$

Inserting the required torque of (2) into the available torque in (4), differentiating with respect to N, and setting the result to zero yields the gear ratio (N^*) that allows for the minimum K_t (and thus the minimum required K_m):

$$N^* = \sqrt{\frac{\left(J_L\alpha_p + 2T_L\right)\left(VI_{\max} - 4J_L\alpha_p\omega_p\right) - 4T_L^2\omega_p - VI_{\max}T_L}{VI_{\max}J_m\alpha_p}} \tag{5}$$

The corresponding value of K_m may be derived by inserting (4) and (5) into (3). By expanding the resulting equation and manipulating J_m to the left-hand side of the equation, it may be seen that:

$$\frac{\left(K_m^*\right)^2}{J_m} = \Phi\left(T_p, \omega_p, \alpha_p, V, \mathrm{I}_{\max}\right), \tag{6}$$

This relationship between K_m and J_m is equivalent to the speed rate (SR) benchmark [8], in which

$$SR = \frac{K_T^2}{J_m R} = \frac{K_m^2}{J_m} = \frac{PR}{I^2 R} = \frac{1}{\tau_m}, \tag{7},$$

where τ_m is the mechanical time constant. The SR value of a motor is independent of winding or battery supply values, and incorporates many of the other benchmarks (K_m, K_t, J_m, and the ratio of power rate to resistive dissipation) [8]. SR's equivalence with (6) suggests that SR provides a valid benchmark that incorporates a motor's ability to produce a single speed/acceleration/torque snapshot on a given profile.

C. *Simulink model for optimization and benchmark testing*

In order to test the hypothesis that SR is the best available benchmark of motor performance, as well as to optimize tuning variables within a given motor, a model was created

based on commercially available motors and tested over a series of tasks.

1) Model

A Matlab[1] based Simulink model (Fig. 3) using a variable-step Dormand-Prince solver was designed that included motor parameters (wire resistance R and inductance L, K_t, rotor viscosity and inertia), transmission parameters (gear ratio and inertia), and load parameters (inertia, torque, and viscosity). Power supply nonlinearities included voltage-saturation set to the supply voltage value and current saturation set to 8 amperes to model batteries in existing prostheses.

The transmission was modeled as a 10:1 planetary friction gear in combination with a cycloid gear, which have low inertia and relatively constant high-efficiency over a wide range of gear ratios and applied speed and torque [11]. Inertia of the planetary friction gear was equal to $3e^{-9}$ kg-m^2 as calculated from the motor shaft. Inertia of the input components of the cycloid was equal to $6e^{-8}$ kg-m^2 as calculated from the cycloid input, and was reflected by 10^{-2} through the planetary friction gear to the motor shaft. Inertia of the cycloid output was $6e^{-6}$ kg-m^2, and was reflected by N^{-2} to the motor shaft. Load parameters were also reflected before the gear ratio to preserve causality and streamline processing. Load viscosity was arbitrarily set to $5e^{-4}$ Nm/(rad/sec), equivalent to the maximum motor viscosity.

2) Tuning ranges

Four supply voltages were examined in 3.7V increments from 3.7V to 14.8V. Thirty-seven brushless DC motors (Emoteq[2] HT0800-HT3005) were analyzed, with SR ranging from 0.2 kHz to 1.8 kHz, K_m ranging from 0.004 to 0.36 Nm/sqrt(Watt), outer diameters ranging from 20 to 76 mm, and lengths ranging from 18 to 76 mm. Motor mass, inertia, and viscosity were updated for each motor. Winding resistance was tuned using 31 bins over a range of 0.001Ω to $2R_{apx}$. Inductance and K_t were appropriately scaled from the original motor windings to match the tuned resistance values using the relationships described below in section II.C.3).

Twenty-two gear ratios were analyzed, including sixteen exponential increments from 20:1 to 400:1 ($N=20+6e^{0.14(i-1)}$), as well as additional ratios of [1 5 10 800 1200 1600]:1. The exponential range of gears may be packaged in a prosthetic device using a friction planetary gear and a single-stage cycloid gear, thus ensuring equal mass and efficiency over the range of analyzed gear ratios. The lower and higher gear ratios were included to provide a better understanding of winding/gear ratio optimization space.

Plant gain was originally set to 1. It was iteratively increased by factors of 5 until the maximum deviation from the position trajectory was less than 5% or until the plant gain had exceeded a threshold of 500,000. The feedback gain equaled *1+Ds*. For each plant gain, D was iteratively calculated from the feedback model's transfer function to produce the minimum imaginary pole component.

3) Tuning parameters

Motor windings may be tuned by changing the diameter of the wire. Changing the diameter of the wire will change the number of turns of wire that will fit in a given slot space, affecting the wire length. These changes will alter the winding resistance R, inductance L, and K_t. Many combinations of R, L, and K_t may exist by tuning the wire diameter, but these three variables are dependent on each other for a given motor, and thus equations must be provided to make sure their dependence is constrained.

The torque constant (K_t) is proportional to the number of turns (Z):

$$K_t = k_w \frac{2}{3} \frac{Z\Phi}{\lambda\pi} \frac{P}{2}, \tag{8}$$

in addition to several other parameters that are independent of the windings: P is the number of poles (magnets), λ is the pole-arc to pole-pitch ratio, and the 2/3 coefficient reflects the fact that 2 out of 3 phases are in use at a time for a 3-phase brushless motor [12]. The flux / pole (Φ) is equal to the open-circuit flux density times the area of the magnet. The torque constant may be represented as $s_Z K_{t0}$ for the purposes of tuning, where K_{t0} is the original torque constant provided by the manufacturer and s_Z is a scaling coefficient proportional to the number of turns.

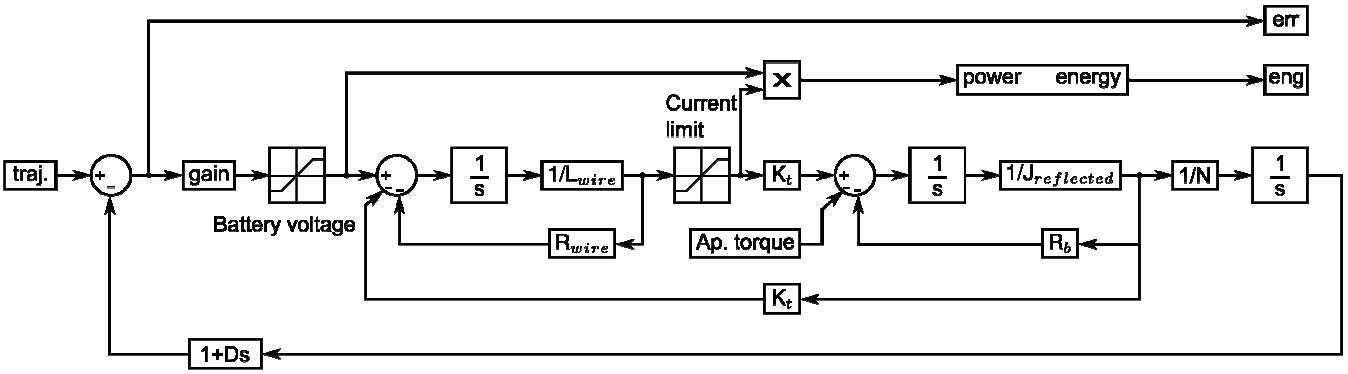

Fig. 3. Simulink model of motor, with feedback control and environmental load/inertia. The model includes voltage and current saturation nonlinearities, and outputs the position error and positive (non-regenerative) energy used.

[1] Matlab is a product of Mathworks, Natick, Massachusetts

[2] Emoteq, Inc.is a division of Allied Motion, Tulsa Oklahoma

The resistance of the windings is influenced both by the diameter and the length of the wire $\left(R = \rho l / A\right)$, where ρ is the resistivity, l is the length, and A is the cross-sectional area of the wire. The diameter of the wire may be calculated as:

$$D = \sqrt{\frac{4F_s F_i A_s}{\pi Z / q}} \tag{9}$$

where F_s is the fill factor (typically equal to 0.3 – 0.35), F_i is the insulation factor (typically equal to 0.8-0.9), A_s is the area in the slot, and q is the number of slots [12]. The length of the windings in a coil equals the length of a single turn (l_c) times the number of coils per slot (Z/q), and the length of the windings across the terminals equals 2/3 the total number of slots times the length of a single coil. The resistance may thus be calculated as

$$R = \frac{2}{3q}\frac{4\rho l_c Z^2}{\pi F_s F_i A_s} \tag{10}$$

and simplified for the purposes of tuning as $s_Z^2 R_0$. It may be seen that the relationship between (8) and (10) is consistent with 3). The inductance of the windings may be expressed as

$$L = \frac{\mu K Z^2 A}{lq} \tag{11}$$

for single layer windings, in which μ_0 is the permeability of the core, K is the Nagaoka coefficient [13], A is the area of the cross-section of the coil, and l is the length of the coil. For multilayer coils, it may be approximated as:

$$L = \frac{0.8 r^2 Z^2}{q\left(6R + 9L + 10d\right)} \tag{12}$$

where r is the mean radius of the coil and d is the depth of the coil, equal to the outer radius minus the inner radius. All length parameters (r, l, and d) in (12) must be in inches.

In either case, the inductance is proportional to Z^2, and may be expressed as $s_Z^2 L_0$.

Thus, for the purposes of tuning, the dependency of K_t, R, and L on the number of winding turns may be expressed as:

$$\begin{aligned} K_t &= s_Z K_{t0} \\ R &= s_Z^2 R_0 \\ L &= s_Z^2 L_0 \end{aligned} \tag{13}$$

where s_z may be tuned to optimize windings based on manufacturer specifications (K_{t0}, R_0, L_0).

4) Other benchmark metrics

Many commonly used metrics are winding-dependent variables that become proportional to winding independent variables when constrained. T_s may be thought of as the winding-dependent daughter of K_m, and $T_{s\,max}$ is proportional to K_m. Likewise, power rate (PR) may be thought of as the winding-dependent daughter of SR. Maximum acceleration equals K_m/J_m, and thus incorporates both torque and inertial characteristics in a winding-independent metric. Maximum power is inversely proportional to the resistance for a fixed voltage, and is thus winding-dependent. Maximum rated continuous power, however, is winding independent. Thus, for the purposes of this analysis, winding independent metrics of SR, K_m, $accel_{max}$, and maximum continuous power rating were used.

TABLE 1
TASKS FOR OPTIMIZATION

Joint	Task	ROM *deg*	t_f *s*	Cycles/day	J_L *kg m²*	T_L *Nm*
Elbow	E1	70	5	20	0.191	10
	E2	100	3	50	0.145	5
	E3	140	1.5	1000	0.104	0.5
Hand	H1	0	0.5	100	0.023	6
	H2	45	0.4	100	0.023	1.4
	H3	60	0.2	4000	0.023	0
Extreme	X1	60	0.02	*N.A.*	0.207	0

5) Simulation Tasks

Models of two prosthetic joints (elbow & hand) were each analyzed for three tasks (Table 1). Only flexion movements were analyzed, because extension movements for each task had applied load torques less than or equal to flexion torques. Load inertia (J_L) was proportional to load torque (T_L) for the elbow and included the measured inertia of a prosthetic arm (0.1 kg-m^2), modeling the loads as point masses applied at the hand 0.3m from the joint axis. Load inertia was constant for the hand. ROM for both joints reflected existing commercial devices and the ROM used in activities of daily living, as did task completion time (t_f) [1]. Task E1 moved a heavy load, whereas H1 applied a stall torque against a non-deformable object. The other tasks for both joints moved decreasingly smaller torques over a decreasing task completion time and increasing ROM.

An additional extreme task (X1) was constructed that did not correspond to typical ADLs. This task was designed to ensure that roughly half of the motors failed to complete the task, in order to compare the ability of performance metrics to predict motor success.

The error in trajectory was measured for each task to ensure that the maximum deviance from the desired trajectory was less than 5% of the ROM. For the case of H1, in which ROM equaled 0, success was defined by less than 0.125° movement in response to the applied torque. Positive electrical power consumed by the motor was summed over time to obtain the energy required to perform the tasks.

For the purposes of motor rating and voltage optimization, consumed energy was converted to mass using the density of lithium-ion batteries (25 g/W-hr per cell, 3.7V/cell). Motors that required different amounts of energy could accordingly be compared to find the lightest weight motor-battery package that was able to accomplish all three tasks for a given joint.

6) Data Analysis

The ability of metrics to predict motor success for a given task was assessed by looking at the Receiver Operator Characteristics (ROC) curve, which reports the true positive rate of prediction vs. the false positive rate of prediction as the discrimination threshold is varied. Metrics with better

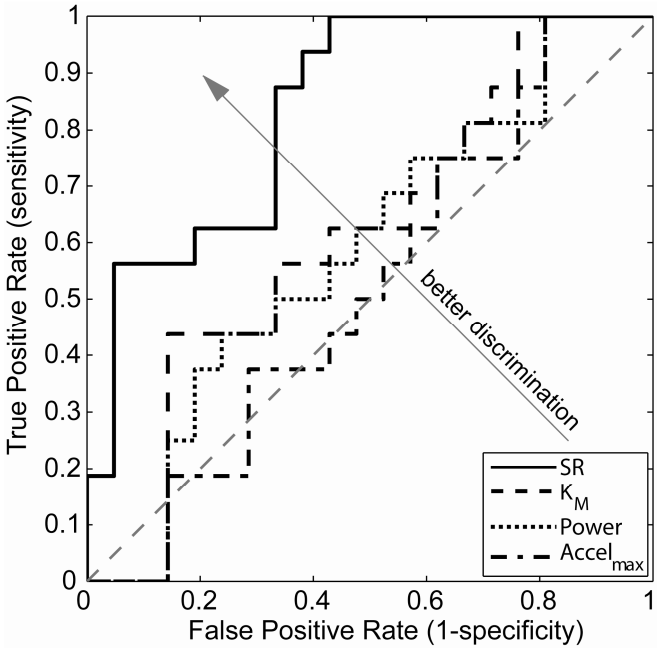

Fig. 4. ROC plot of Performance metrics.

discriminatory power have an ROC curve closer to the left and top edges of the plot, signifying that they have a high true positive rate and a low false positive rate. Area under the curve (AUC) was also reported. An AUC of 50% signifies no discriminatory power and an AUC of 100% signifies perfect discriminatory power.

Correlation between the metrics and minimum energy expenditure was assessed using the r^2 statistic, which reports the percent of the variability in energy expenditure explained by the metric, and the root mean square error (RMSE) of the model, which reports how well the model fits the data.

The ability of metrics to predict the optimal winding across motors and tasks was assessed by measuring the consistency of the metric across motors and the seperability of the metric across tasks. Consistency was defined as the standard deviation of the metric across motors for a given task, and low values were desirable – indicating that the metric was consistent across motors. Seperability was defined as the standard deviation of the metric across tasks for a given motor, and high values were desirable – indicating that the metric suggested different windings for different tasks. The dimensionless tuning information ratio was defined as the average seperability divided by the average consistency, and larger ratios signified better tuning metrics.

III. Results

A. Motor Performance Metrics

1) Motor failure test using the extreme task

The extreme task was simulated over a voltage range of 20-60V in 10V increments to find a voltage at which approximately half of the motors failed. A voltage of 30V caused 21 of the 37 (57%) motors to fail over the entire

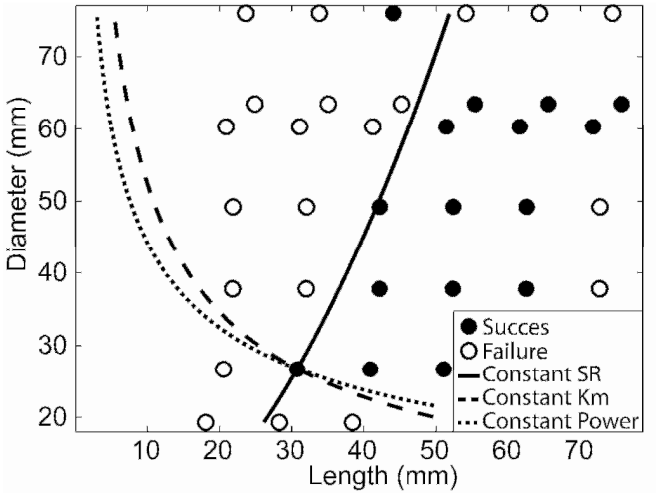

Fig. 5. Motor success/failure projected onto motor length and outer diameter. Curved lines with constant SR, K_m, and power are shown.

range of tested windings and gear ratios. Of the four metrics assessed, speed ratio (SR) was the best predictor of motor success (Fig 4), with an AUC of 77%, followed by K_m (61%), rated power (59%), and maximum acceleration (52%). Due to the low predictive power of maximum acceleration, it is omitted from the rest of the paper, although its inclusion here should demonstrate that SR contains more information than an acceleration value.

a) Length vs. Diameter

The dependency of SR on motor length L_n and outer diameter OD for the motors was fit using a Moore-Penrose pseudoinverse [14]. Doing so yielded the following relationship

$$SR \propto \frac{L_n}{\sqrt{OD}} \tag{14}$$

This relationship suggests that SR (and by inference from the preceding section, motor performance), improves with decreased diameter. This relationship is in contrast to $K_m \propto OD^2$ and $power \propto OD^{1.7}$.

To visualize this observation, motor success/failure was plotted vs. length and outer diameter. Metrics with a constant value as a function of length and diameter were overlaid on this plot to visualize the effect of metric prediction as it related to the geometry of the motor (Fig. 5). A constant SR value was more reflective of the motor boundary space than either a constant K_m value or a constant power value, although none of the metrics accurately captured the failed motors in the right-hand portion of the plot.

2) ADL Energy minimization

All of the motors were able to complete the set of three tasks for each joint for at least one set of voltage, winding, and gear ratio parameters. The minimum energy was calculated among those points in this space that successfully completed all three tasks. The resulting energy was fit as a function of performance metrics after removing outliers using Grubb's test (α=0.1). For the set of elbow tasks, K_m was the best

representative of expended energy (Table 2), followed by rated power and SR. For the set of hand tasks, SR was the best representative of expended energy. The other two variables (K_m and power rating) had minimal correspondence with energy expenditure (r^2<0.1).

Task H1 was a stall-task, and as such did not involve movement. As a result, SR would not be expected to correlate better than K_m for H1. The metrics were accordingly fit as well with tasks H2-H3, both of which involved movement. SR provided even stronger correlation for H2-H3 (r^2=0.73, RMSE=148 mW-hr), followed by K_m and rated power (r^2=0.3, RMSE=238 mW-hr).

Motors with higher SR, K_m, or power rating, although generally reducing the energy expenditure, also result in increased motor mass. At some point the reduced energy mass intersects the increased mass of the motor, resulting in a minimum total mass. This intersection is a function of the metric densities, the battery densities, and the set of ADLs.

B. Winding and gear ratio optimization

Four metrics were assessed regarding their ability to maintain a constant value across different motors (consistency), while providing different values across tasks (seperability), using the tuning information ratio defined in II.C.6). These metrics included winding resistance R and three winding-dependent metrics: T_s, $accel_{max}=T_s/J_m$, and $PR = T_s^2 / J_m$. Winding resistance R provided the highest tuning information ratio (1.04), followed by values of 0.70, 0.24, and 0.22 for PR, $accel_{max}$, and T_s.

The minimum-energy winding/gear combination for a given motor was typically in the middle of the acceptable combinations, both for single tasks and across tasks for a given joint (Fig. 6). The minimum-energy combination usually had a winding with resistance less than $R_{apx}=V/I_{bat}$, although windings above this resistance often produced acceptable trajectories.

One exception to resistances being less than R_{apx} was for the stall-torque task, in which maximum gear ratios allowed the required torque to be relatively small. Given such a small torque, minimum energy was expended when resistance was maximized (making that point the stall torque of the motor). Even though such motors had low stall torque and were unable to move efficiently, they were able to generate the required torque with low energy requirements.

If the gear ratio was allowed to vary between tasks (quasi continuously variable transmission (CVT)), and could range between 1:1 and 1:12, a total of 25g was saved for the set of hand ADLs. Thus, a CVT would have to weigh less than 25g and have a range of at least 1:1 to 1:12 to merit inclusion in such a design.

TABLE 2

Predictive power of performance metrics to model total energy consumed over course of ADLs.

	E1-E3		H1-H3	
	r^2	RMSE *mW-hr*	r^2	RMSE *mW-hr*
SR	0.09	169	0.55	217
K_m	0.40	138	0.09	309
Rated Power	0.35	143	0.05	315

C. Voltage optimization

Although there was an optimal voltage level for each motor that minimized energy expenditure (typically 11.1V), energy expenditure for each of the tasks across voltage levels varied less than the associated increase in weight needed to increase the voltage (25 g/mW-hr per cell). Thus, the minimum-cell battery that could accomplish a task (7.4V) always resulted in the lowest total-mass system.

IV. Discussion

SR provided a useful metric in deciding whether a motor would fail to perform a task. Although SR is often thought of solely as a responsiveness variable because it is inversely proportional to the mechanical time constant, it must be emphasized that SR is proportional to K_m^2, and thus provides important information regarding the torque-producing capabilities of the motor. As shown in the methods section (6), SR captures the torque, speed, and acceleration requirements at a given voltage and current level. At a conceptual level, SR thus seems better posed to assess motor success than either K_m or rated power.

SR should theoretically have had a perfect ROC curve for prediction of motor success. The model used in this study used position feedback, and defined success as less than 5% position error. Several motors were able to achieve this positional accuracy while having phase-lag between intended velocity and acceleration, resulting in substantially smaller generated SR values than the values required by the actual trajectory. Thus the failure of SR to provide a perfect ROC curve is more likely the result of the simulation model than the metric.

SR had a higher correlation with energy consumption for the hand tasks than the other metrics, but lower correlation for the elbow tasks. The hand tasks required higher

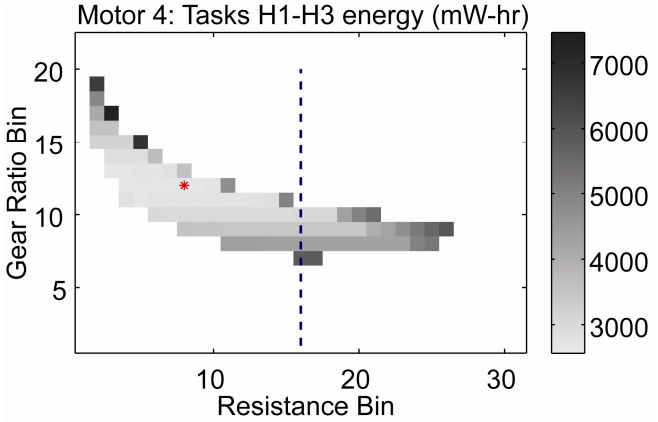

Fig. 6. Example of the gear ratio / winding space for the combined set of hand ADLs. The line represents R_{apx} = Vbat/Ibat. The asterix represents the minimum-energy combination.

accelerations than the elbow tasks, which may account for the better correlation between SR and energy expenditure.

These simulations suggested that narrow, longer motors provided better performance than short, large-diameter motors, provided an acceptable gear ratio was available. This result is in contrast both with conventional theory, in which diameter is maximized to increase torque capabilities [15], as well as several existing anthropomorphic robotic applications [4, 6], but is a reasonable guide once the inertia of the motor is incorporated into calculations. Once the added inefficiency of the gear train is included, however, short, large diameter motors still excel in many tasks.

Gear-ratio dependent inefficiency was not included in this study. This is an appropriate simplification for use of some transmissions, such as cycloid drives [11], but not appropriate if using other transmissions such as stacked planetary gear stages. The influence of gear inefficiency on stacked planetary gear stages could be added as follows:

$$T_{pGR} = \frac{T_p + T_c \Big/ \prod N}{\eta}$$

$$\eta = \eta_0^q \qquad , \qquad (15)$$

$$T_c = \sum_{i=1}^{q} \left[T_{co} \eta_0^i \prod_{k=q-i+1}^{q} N(k) \right]$$

where η_0 is the torque-dependent efficiency coefficient per stage, q is the number of stages in the stack, T_{co} is the stiction torque per stage, and N is an array of the gear ratio of each stage. η may not easily be extracted to act as a compensation coefficient for K_m or SR.

Recent studies [6] have shown that the introduction of compliance can increase the speed of robots for a given torque/inertia profile. A metric that incorporated this ability along with the characteristics of SR would provide a useful metric for future robotic motor optimization.

V. Conclusion

SR provides a mathematically well-posed description of the torque, speed, and acceleration requirements of a given point within a trajectory, and provides a better metric than motor constant K_m or rated power in predicting motor success. Optimizing windings to minimize energy expenditure results in a robust winding that is not prone to task-failure. Voltage should always be minimized to the lowest level at which the task may be completed in order to minimize weight.

Acknowledgment

The author thanks Lalith Wickramarathna for his initial literature review of motor design, Dr. Jackrit Suthakorn and the BART laboratory of Mahidol University for their support, members of RIC, including Nate Bunderson, Todd Kuiken, Aimee Schultz, and Richard Weir, for their review and processing insights, and Dr. Miller and Mr. Hendershot for their helpful correspondence regarding motor design.

Appendix

If I_{max} is limited by the resistance of the windings (Fig. 2, right side; $I_{max} = V/R$), then I_{max} is dependent on K_t. In this case (1) may be reformulated as

$$T = K_m^2 \left(\frac{V}{K_t} - N\omega_p \right). \qquad (16)$$

Rearranging (16) we may solve for K_t:

$$K_t = \frac{VK_m^2}{T + N\omega_p K_m^2} \qquad (17)$$

Following the same steps used to derive (5), the gear ratio necessary to minimize K_t and K_m may be found as:

$$N^* = \sqrt{\frac{J_L \alpha_p + T_L}{J_m \alpha_p + K_m^2 \omega_p}} \qquad (18)$$

References

[1] C. W. Heckathorne, "Components for electric-powered systems," in *Atlas of Amputations and Limb Deficiencies*, 3 ed Rosemont, IL: American Academy of Orthopaedic Surgeons, 2004, pp. 145-172.

[2] S. C. Jacobsen, M. Olivier, F. M. Smith, D. F. Knutti, R. T. Johnson, G. E. Colvin, and W. B. Scroggin, "Research robots for applications in artificial intelligence, teleoperation and entertainment," *International Journal of Robotics Research,* vol. 23, pp. 319-330, Apr-May 2004.

[3] A. M. Dollar and H. Herr, "Lower extremity exoskeletons and active orthoses: Challenges and state-of-the-art," *IEEE Transactions on Robotics,* vol. 24, pp. 144-158, Feb 2008.

[4] J. W. Sensinger and R. F. f. Weir, "User-Modulated Impedance Control of a Prosthetic Elbow in Unconstrained, Perturbed Motion," *IEEE Transactions on Biomedical Engineering,* vol. 55, pp. 1043-1055, 2008.

[5] G. Puchhammer, "Future actuating technologies for upper-extremity prosthetic devices," in *10th International Conference on New Actuators* Bremen, Germany, 2006, pp. 301-307.

[6] A. Albu-Schaffer, O. Eiberger, M. Grebenstein, S. Haddadin, C. Ott, T. Wimbock, S. Wolf, and G. Hirzinger, "Soft robotics - From torque feedback-controlled lightweight robots to intrinsically compliant systems," *IEEE Robotics & Automation Magazine,* vol. 15, pp. 20-30, Sep 2008.

[7] J. M. Hollerbach, I. W. Hunter, and J. Ballantyne, "A comparative analysis of actuator technologies for robotics," in *Robotics Review 2* Cambridge, MA: MIT Press, 1991, pp. 299-342.

[8] T. J. E. Miller, *Speed's electric motors: an outline of some of the theory in the speed software for electric machine design with problems and solutions*. Hillsboro, OH: Magna Physics Publishing, 2006.

[9] R. F. Weir, M. Mitchell, S. A. Clark, G. Puchhammer, K. Kelley, M. Haslinger, N. Kumar, R. Hofbaur, P. Kuschnigg, V. Cornelius, M. Eder, and R. Grausenburger, "New Multifunctional Prosthetic Arm and Hand Systems," in *International Conference of the IEEE Engineering in Medicine Society* Lyon, France, 2007, pp. 4359-4360.

[10] T. Flash and N. J. Hogan, "The coordination of arm movements: an experimentally confirmed mathematical model," *Journal of Neuroscience,* vol. 5, pp. 1688-1703, 1985.

[11] J. W. Sensinger, "Unified approach to cycloid drive profile, stress, and efficiency optimization," *ASME Journal of Mechanical Design,* vol. MD-09-1060: Accepted for publication, 2010.

[12] J. R. Hendershot and T. J. E. Miller, *Design of brushless permanent-magnet motors*. Hillsboro, OH: Magna Physics Publishing, 1994.

[13] H. Nagaoka, "The inductance coefficients of solenoids," *Journal of the College of Science, Imperial University, Tokyo, Japan,* vol. 27, pp. 1-33, 1909.

[14] G. H. Golub and C. F. Van Loan, *Matrix computations*, 3rd ed. Baltimore: Johns Hopkins University Press, 1996.

[15] H. Asada and K. Youcef-Toumi, *Direct-drive robots: theory and practice*. Cambridge, MA: MIT Press, 1987.